MDPI

Article

A Deep Learning Approach for Gait Event Detection from a Single Shank-Worn IMU: Validation in Healthy and Neurological Cohorts

Robbin Romijnders[1]*, Elke Warmerdam[2], Clint Hansen[1]*, Gerhard Schmidt[3] and Walter Maetzler[1]

[1] Department of Neurology, Kiel University, 24105 Kiel, Germany; r.romijnders@neurologie.uni-kiel.de (R.R.), c.hansen@neurologie.uni-kiel.de (C.H.), w.maetzler@neurologie.uni-kiel.de (W.M.)
[2] xxxxx, xxxxx, xxxxx Homburg, Germany; elke.warmerdam@uni-saarland.de (E.W.)
[3] Institute of Electrical Engineering and Information Technology, Faculty of Engineering, Kiel University, 24143 Kiel, Germany; gus@tf.uni-kiel.de (G.S.)
* Correspondence: r.romijnders@neurologie.uni-kiel.de (R.R.)

Abstract: A single paragraph of about 200 words maximum. For research articles, abstracts should give a pertinent overview of the work. We strongly encourage authors to use the following style of structured abstracts, but without headings: (1) Background: place the question addressed in a broad context and highlight the purpose of the study; (2) Methods: describe briefly the main methods or treatments applied; (3) Results: summarize the article's main findings; (4) Conclusions: indicate the main conclusions or interpretations. The abstract should be an objective representation of the article, it must not contain results which are not presented and substantiated in the main text and should not exaggerate the main conclusions.

Keywords: keyword 1; keyword 2; keyword 3 (List three to ten pertinent keywords specific to the article; yet reasonably common within the subject discipline.)

Citation: Romijnders, R.; Warmerdam, E.; Hansen, C.; Schmidt, G.; Maetzler, W. A Deep Learning Approach for Gait Event Detection from a Single Shank-Worn IMU: Validation in Healthy and Neurological Cohorts. *Sensors* **2022**, *1*, 0. https://doi.org/

Received:
Accepted:
Published:

Publisher's Note: MDPI stays neutral with regard to jurisdictional claims in published maps and institutional affiliations.

1. Introduction

Gait deficits are common in older adults and possibly reflect the presence of an underlying neurodegenerative disease [1,2]. For example, conversion to Parkinson's Disease [3] or from mild cognitive impairment to Alzheimer's Disease [4,5] are linked with changes in spatiotemporal gait parameters. Similarly, temporal gait parameters are different for stroke patients [6,7] and patients with multiple sclerosis [8,9] when compared to healthy controls. To objectively quantify gait deficits, stride-specific parameters such as stride time or stride length are often used [10], where the beginning and end of a stride are determined from two successive initial contacts (ICs) of the same foot [11,12]. The IC is when the foot contacts the ground and together with the instant at which the foot leaves the ground (final contact, FC), each stride can be divided in a stance and swing phase [13,14]. The events of IC and FC, also referred to as *gait events*, are commonly determined using force or pressure measuring devices [14], or passive, retro-reflective marker-based optoelectronic motion capture systems (henceforth referred to as the *marker-based* system or method) [15,16]. These systems are relatively expensive, and restricted to usage in expertise laboratories [17,18]. As there is increasing evidence that gait measured in the lab does not reflect daily-life gait [19–21], there is more and more interest in measurement systems that allow for continuous gait analysis in ambulatory settings. Therefore, the use of inertial measurement units (IMUs) is especially attractive, as these can be used to measure gait in ecologically valid environments, such as the home environment, thereby painting a more complete picture of health status [22,23] and providing clinical information that is complementary to standardized lab-based assessments [20,21,24,25].

Previous research suggests that gait event detection is more accurate using an IMU worn on a lower limb (e.g., shank or foot) compared to an IMU worn on the low back [26–28].

Now, in order to get from abstract IMU sensor readings to clinically relevant gait parameters (e.g., from accelerations and angular velocities to stride times) [10], different algorithmic approaches have been developed in the last twenty years of clinical gait research. A recent study has evaluated a cross-section of these algorithms for different sensor locations on the lower leg and foot [29]. The algorithms were categorized according to which signals were analyzed, for example the angular velocity about the medio-lateral axis, or the accelerations along vertical and antero-posterior axis. This means the sensor readings need to be linked with the anatomical axes, that is, one needs to know which sensor axis aligns with for example the medio-lateral axis. In most approaches, it is simply assumed that due to sensor attachment the sensor axis aligns roughly with the anatomical axis of interest ([30–36]) or an additional calibration procedure (e.g., [37]) is required ([29,38]). In ambulatory assessments however, study participants often attach the sensor themselves, and therefore the sensor location and alignment cannot be controlled for. Furthermore, it is unlikely that each time the sensor is (re-)attached study participants, especially those with gait deficits, perform a calibration procedure that usually consists of holding a pre-defined pose and performing some known movement sequences (TODO: reference?! Kong? Seel?).

Taken together, this drives the need for an approach that is invariant to sensor orientation, and is applicable across a variety of pathological gait patterns. As pointed out by [10], in the field of image analysis similar requirements have been successfully addressed by algorithms that share a common underlying methodology referred to as deep learning [39,40]. Recent applications of deep learning algorithms have already shown improved performance in detecting gait events from marker-based motion capture when compared to conventional, often heuristics-based, algorithms [41–43]. Another study used a deep learning approach to detect gait events from either three IMUs (worn on the low back, and both ankles) or a single IMU (worn on the low back), and showed that the time error was considerably smaller for the deep learning algorithm than for a commonly applied wavelet-based approach [44].

In this study, we further these works by validating this deep learning approach for detecting gait events in a heterogeneous cohort of healthy and neurologically diseased adults considering a single IMU setup, worn on the lower leg.

2. Materials and Methods

2.1. Data Collection

Gait analyses were performed in the Universitätsklinikum Schleswig-Holstein (UKSH) campus Kiel, Germany. The study [45] was approved by the ethical committee of the medical faculty at the UKSH (no: D438/18). In total, data from 160 participants were included for the current analysis, including data from young adults (YA; age: 18 - 60 years), older adults (OA; age: >60 years), people with Parkinson's Disease (PD; according to the UK Brain Bank criteria [46]), people with a recent (<4 weeks) symptomatic stroke (stroke), people with multiple sclerosis (MS; according to the McDonalds criteria [47]), people with chronic low back pain (cLBP), and people with other diagnoses that were assumed not to affect mobility (Table 1). Inclusion criteria were an age of 18 years or older, and the ability to walk independently without a walking aid. Participants were excluded from the study with a Montreal Cognitive Assessment [48] score <15 and other movement disorders that affected mobility, as noticed by the clinical assessor.

Table 1. Demographics data of the study participants. Age, height, and weight are presented as mean (standard deviation).

Group	Gender	Number of subjects	Age years	Height cm	Weight kg
YA	F	21	27 (7)	173 (5)	67 (8)
	M	22	30 (9)	185 (8)	81 (13)
OA	F	11	70 (6)	167 (6)	72 (17)
	M	11	73 (6)	180 (6)	83 (11)
PD	F	12	67 (6)	168 (6)	70 (14)
	M	20	62 (11)	178 (6)	87 (13)
MS	F	12	37 (9)	174 (9)	75 (9)
	M	9	42 (15)	189 (8)	96 (30)
stroke	F	4	66 (10)	160 (6)	65 (11)
	M	17	67 (17)	178 (7)	84 (14)
cLBP	F	3	64 (10)	166 (5)	65 (5)
	M	7	63 (16)	178 (7)	90 (16)
other	F	3	60 (13)	166 (3)	79 (15)
	M	8	68 (18)	182 (7)	85 (13)

Group: YA: younger adults, OA: older adults, PD: Parkinson's Disease, MS: multiple sclerosis, cLBP: chronic low back pain; **Gender**: F: female, M: male.

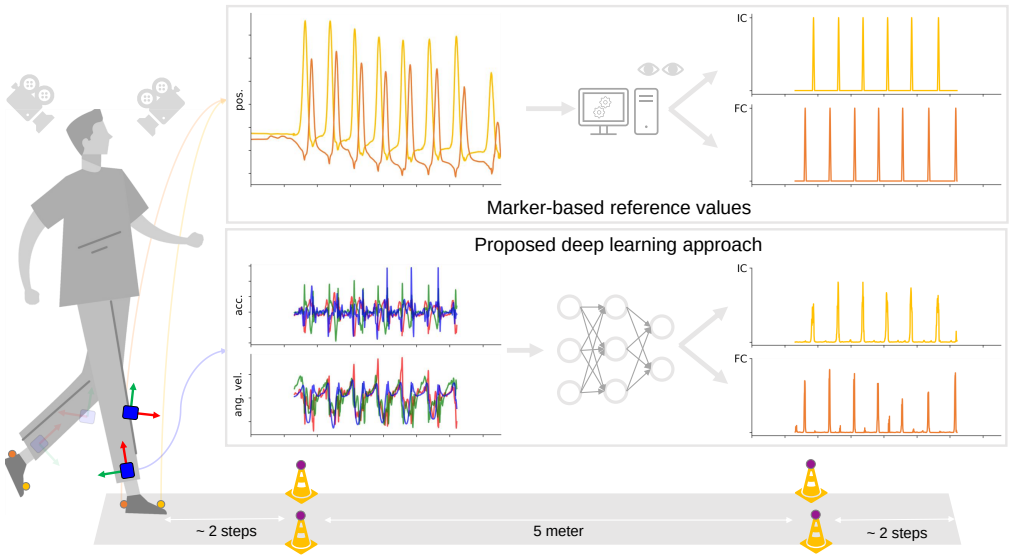

Figure 1. Schematic depiction[1] of the current study. Study participants wore IMUs on the ankle and shanks, and reflective markers were adhered on the heel and toe of usual footwear (shown on the left). Marker data were used to obtain reference values for the timings of initial and final contacts (top), where accelerometer and gyroscope data from each tracked point were inputted to a neural network that predicted timings of the same initial and final contacts (bottom).

[1] Picture from: https://www.vecteezy.com/free-vector/man-walking.

Participants performed three walking trials consisting of walking 5 meter at either (1) preferred speed ("*Please walk at your normal walking speed.*"), (2) slow speed ("*Please walk half of your normal walking speed.*"), or (3) fast speed ("*Please walk as fast as possible, without running or falling.*"). The 5 meter distance was marked with two cones on both ends, and participants were asked to start walking approximately two steps before the cones on one end, and stop walking approximately two steps after passing the cones on the other end.

For the current analysis data from four IMUs (Noraxon USA Inc., myoMOTION, Scottsdale, AZ, USA) were considered, namely those that were attached laterally above the left and right ankle joint and those attached proximally at the left and right shank. IMUs were secured to participants using elastic bands with a special hold for the IMU. Furthermore, reflective markers were attached on top of the usual foot wear at the heel and toe of both feet (Figure 1). Marker data were recorded using a twelve-camera optoelectronic motion capture system (Qualisys AB, Göteborg, Sweden) at a sampling frequency of 200 Hz. IMU data were recorded at the same sampling frequency, and both systems were synchronized using a TTL signal [45]. For some recordings, the sampling frequency of the IMUs was erroneously set at 100 Hz, and therefore data from these trials were upsampled before further analysis.

2.2. Data Pre-processing

2.2.1. Marker Data

The reflective marker data were first used to determine start and end of each trial. The start of the trial was defined as the time for which the first toe marker (left or right) crossed the *virtual* starting line. The end was defined as the time for which the last heel marker crossed the end line. For both marker and IMU systems, data were then cropped from start to the end of the trial.

Any remaining gaps in the marker data were filled by interpolation making use of inter-correlations between markers [49,50]. The data were then low-pass filtered using a double pass 6th order Butterworth filter with a cut-off frequency of 20 Hz [51,52]. The filtered data were differentiated to get velocity signals, and timings of ICs and FCs were determined from local maxima and minima in the heel and toe vertical velocity signals [53,54]. Like in [34,55], all identified ICs and FCs were manually checked, and corrected if necessary, using Qualisys Track Manager 2018.1 software (Qualisys AB, Göteborg, Sweden). The resulting annotated ICs and FCs were considered the *true* events (also *labels* or *targets*), and were used as reference timings to derive stride-specific gait parameters.

2.2.2. IMU Data

The idea behind the deep learning approach was that a *model* was trained to predict the likelihood of an IC and FC, given accelerometer and gyroscope data from a single IMU. In other words, the model was iteratively trained to learn a mapping $h_{\mathbf{W}}(\mathbf{X}) : \mathbf{X} \rightarrow \mathbf{y}$, where $h_{\mathbf{W}}$ was also referred to as the *hypothesis* parameterized by the weights, collectively denoted by $\mathbf{W}$, $\mathbf{X}$ was the matrix of IMU data, and $\mathbf{y}$ was the vector of annotated events.

Here, the matrix $\mathbf{X}$ consisted of the IMU data, arranged as:

$$\mathbf{X} = \begin{bmatrix} | & | & & | \\ \mathbf{x}_1 & \mathbf{x}_2 & \cdots & \mathbf{x}_D \\ | & | & & | \end{bmatrix} = \begin{bmatrix} x_1[1] & x_2[1] & & x_D[1] \\ x_1[2] & x_2[2] & & x_D[2] \\ \vdots & \vdots & \cdots & \vdots \\ x_1[N] & x_2[1] & & x_D[N] \end{bmatrix}, \quad \mathbf{X} \in \mathbb{R}^{N \times D} \tag{1}$$

where $\mathbf{x}_d = \begin{bmatrix} x_d[1] & x_d[2] & \cdots & x_d[n] & \cdots & x_d[N] \end{bmatrix}^{\mathrm{T}}$, with $d = 1, \cdots, D$ referred to the d-th channel, and $n = 1, \cdots, N$ referred to the n-th sample (or discrete time step).

Accordingly, the vector $\mathbf{y}$ consisted of the annotated events, arranged as:

$$\mathbf{y}_{\mathrm{IC}} = \begin{bmatrix} y_1[1] \\ y_1[2] \\ \vdots \\ y_1[N] \end{bmatrix}, \quad \mathbf{y}_{\mathrm{FC}} = \begin{bmatrix} y_2[1] \\ y_2[2] \\ \vdots \\ y_2[N] \end{bmatrix}, \quad y_i[n] \in [0, 1] \tag{2}$$

The data were split in three independent data sets, namely a training set, a validation set, and a test set. Each set contained data from approximately one-third of the participants.

Participants were randomly assigned to one of the sets, stratified by both group (i.e., diagnosis) and gender (Table 1).

Accelerometer and gyroscope data were normalized by subtracting the channel-wise mean, and dividing by the channel-wise standard deviation. Then, for the training and validation data set, the data were partitioned into equal length time windows [43] of 400 samples, with an overlap of 50% between successive windows (corresponding to 2 s windows, and 1 s overlap, respectively).

2.3. Model

2.3.1. Model Architecture

The basic architecture for the deep learning model was a temporal convolutional network (TCN) [43,57,58]. The TCN consisted of repeating blocks of dilated convolutions (CONV) [56,57] that were followed by batch normalization (BN) [60], rectified linear unit (ReLU) activation, and dropout (DropOut) [61]. For each given dilation factor, the sequence of layers CONV-BN-ReLU-DropOut was repeated twice [58]. Dilation factors were given as a sequence of increasing powers of 2, e.g., $\{1, 2, 4, 8\}$ [56,57,62]. These repeating blocks were followed by a fully-connected (dense) layer with sigmoid activation, and outputs were predicted separately for ICs and FCs. The mean squared error (MSE) was used as loss function, and a gradient descent-based optimization algorithm with adaptive moment (Adam) optimizer was used to iteratively learn the weights [64,65].

2.3.2. Hyperparameter Optimization

In order to find the best model architecture, hyperparameter tuning was perfomed using KerasTuner [63]. Here, the number of filters, the kernel size, and the maximum dilation factor (Table 2) were optimized for using a random search strategy [66].

Table 2. Model hyperparameters that were optimized for, and the corresponding sets of possible values.

Description	Possible values
Number of filters	8, 16, 32, 64, 128
Kernel size	3, 5, 7
Dilations	[1, 2], [1, 2, 4], [1, 2, 4, 8]

The model architecture that resulted from the hyperparameter optimization was then trained on the combined set of training and validation data. The trained model was used to predict occurrence of gait events from the hold-out test set.

2.4. Analysis

The predictions of the model on the test set data were compared with the labels from the test set. The model performance was evaluated for (1) overall detection performance, (2) time agreement between the predicted events and the (marker-based) annotated events, (3) agreement between subsequently derived gait parameters.

2.4.1. Overall detection performance

The overall detection performance quantified how many of the annotated evens were detected by the model (true positives, TP), how many of the annotated events were not detected (false negatives, FN), and how many event that were detected, were actually not annotated (false positives, FP). From these metrics, the recall (or sensitivity), precision and F_1 score were calculated as:

$$\text{recall} = \frac{\text{TP}}{\text{TP} + \text{FN}}$$

$$\text{precision} = \frac{\text{TP}}{\text{TP} + \text{FP}}$$

$$\mathrm{F}_1 \text{ score} = 2 \cdot \frac{\text{recall} \cdot \text{precision}}{\text{recall} + \text{precision}}$$

2.4.2. Time Error

For all correctly detected gait events (TP, Section 2.4.1), the time error between the annotated and detect gait event was defined as:

$$\text{time error} = t_{\text{ref}} - t_{\text{pred}} \tag{3}$$

with t_{ref} the gait event time from the marker-based annotations, and t_{pred} the gait event time from the model predictions. As a robust measure for the average time error and its spread, the median time error and the inter-quartile range (IQR) were reported [70].

2.4.3. Stride Parameters

For those trials for which all gait events were detected, and no spurious events were detected, the stride time, stance time and swing were calculated. Stride was the time between two successive ICs of the same foot. Stance time was the time between FC and the preceding IC of the same foot. Swing time was the time between the IC following the last FC of the same foot.

3. Results

3.1. Overall detection performance

The performance of detecting initial contacts and final contacts was objectively quantified by the number of annotated events that were detected (true positives, TP), the number of annotated events that were not detected (false negatives, FN), and the number of detected events that were not annotated (false positives, FP). From these, recall, precision and F_1 score were calculated (Table 3).

Table 3. Overall detection performance for initial contacts and final contacts as quantified by recall, precision and F_1 score.

	Initial contacts						Final contacts					
Tracked point	**TP**	**FN**	**FP**	**recall**	**precision**	**F1**	**TP**	**FN**	**FP**	**recall**	**precision**	**F1**
left ankle	624	19	5	97%	99%	98%	606	32	10	95%	98%	97%
right ankle	599	42	8	93%	99%	96%	614	17	12	97%	98%	98%
left shank	605	38	15	94%	98%	96%	585	53	18	92%	97%	94%
right shank	603	36	15	94%	98%	96%	595	30	9	95%	99%	97%

TP: true positives, FN: false negatives, FP: false positives, F1: F_1 score.

For both ICs and FCs, recall is high for each of the tracked points (i.e., $\geq$ 92%), and so is precision (i.e., $\geq$ 97%). Differences between the tracked points are small, i.e. the minimum recall is 92% and the maximum recall is 97%, and the minimum precision is 97% and the maximum precision is 99%.

3.2. Time Error

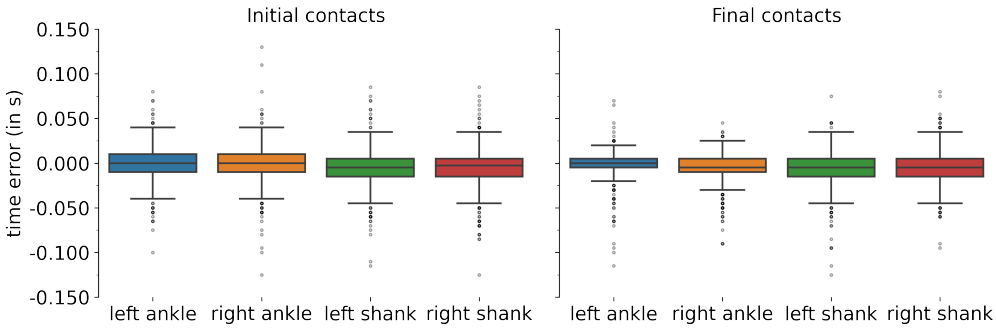

Figure 2. Time errors for initial (left) and final (right) contacts detection, for each of the different tracked points.

Time errors for ICs and FCs are visually depicted using boxplots for each tracked point. Data were not normally distributed, thus Wilcoxon signed-rank tests were used to evaluate whether the median time error was zero.

Table 4. Time errors for the correctly detected gait events.

Tracked point	Initial contacts		Final contacts	
	median	IQR	median	IQR
	s	s	s	s
left ankle	0.000	0.020	0.000	0.010
right ankle	0.000	0.020	-0.005	0.015
left shank	-0.005	0.020	-0.005	0.020
right shank	-0.003	0.020	-0.005	0.020

IQR: inter-quartile range.

3.3. Gait parameters

For those trials for which all gait events were correctly detected (and no spurious events were detected, i.e., no false positives), stride time, stance time and swing time were calculated. The mean difference and the limits of agreement between the NN-derived gait parameters and the marker-based annotations were calculated.

For all stride-specific gait parameters, and for all tracked points, the mean difference compared to the marker-based reference values was close to zero, i.e., the maxmum mean difference was 0.003 s. Furthermore, for all gait parameters and for all tracked points the limits of agreement, based on a 95% confidence interval were distributed around zero with the overall span between -0.049 s and 0.051 s.

Table 5. Time agreement between the stride-specific parameters.

Tracked point	Parameters	Mean difference ms	Limits of Agreement (ms, ms)
left ankle	stride time	0.001	(-0.035, 0.036)
	stance time	0.002	(-0.039, 0.042)
	swing time	-0.001	(-0.045, 0.043)
right ankle	stride time	0.000	(-0.039, 0.040)
	stance time	-0.002	(-0.048, 0.044)
	swing time	0.003	(-0.046, 0.051)
left shank	stride time	0.001	(-0.039, 0.041)
	stance time	0.002	(-0.043, 0.046)
	swing time	-0.001	(-0.049, 0.047)
right shank	stride time	-0.000	(-0.031, 0.031)
	stance time	0.002	(-0.046, 0.049)
	swing time	-0.002	(-0.049, 0.046)

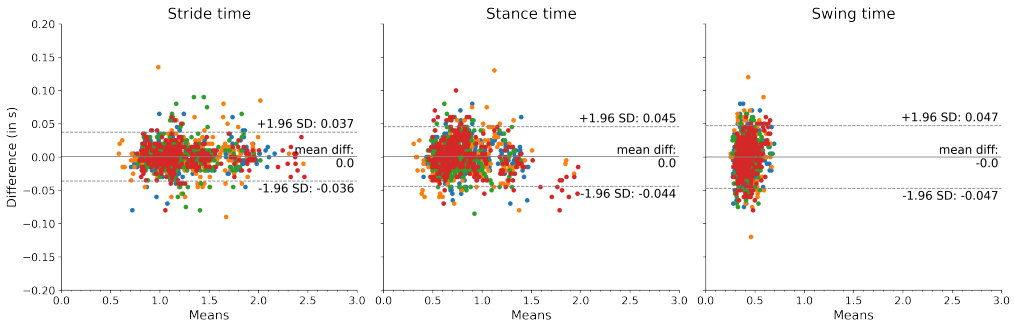

Figure 3. The agreement of extracted gait parameters between the sensor-based and marker-based methods.

4. Discussion

The current study aimed to validate a deep learning approach for detecting gait events from a single IMU worn on the lower leg. Data from left and right ankle- and shank-worn IMUs were used for training a neural network to detect gait events from walking trials performed by healthy younger and older adults, participants diagnosed with Parkinson's Disease, multiple sclerosis, or chronic low back pain, participants who had a recent symptomatic stroke, and participants diagnosed with other neurological diseases. Participants walked a 5 meter distance at three different self-selected walking speeds. The gait event timings that were predicted by the neural network were compared to a common reference method, i.e., stereophotogrammetry, and clinically relevant stride-specific gait parameters were extracted.

A first measure for the model performance was given by the recall (how many annotated events were detected) and precision (how many detected events were annotated). For both initial contacts and final contacts, a high recall ($\geq$ 95%) and high precision ($\geq$ 98%) were observed, meaning that most events can be detected and most detected events were actually true events. There was little difference in recall and precision between tracked points (Table 3) confirming that the deep learning approach is relatively invariant to exact sensor localization. These values for recall and precision were slightly lower than our previously reported 100% [34] that used a heuristics-based approach [30], but in the current study more trials were included and from a more heterogeneous study population.

Next, the time error, that is the difference between the annotated event and the detected event, was of interest. For both initial contacts and final contacts, and for all tracked points, the observed time error was small, and the middle 50% of the time errors were within a

range of $[-0.015, 0.010]$ s (Table 4, Figure 2). These data showed that the deep learning-based is approach is precise in detecting initial and final contacts. Time errors were slightly smaller than our previously reported results [34] that used a heuristics-based approach [30]. The heuristics-based approach determined ICs and FCs as local minima in the medio-lateral angular velocity [30] and it could be that these minima do not exactly coincide with the referent event timing as determined from the stereophotogrammetry.

From the correctly detected gait events, stride-specific gait parameters were derived. These are probably of greatest clinical relevance, as changes in stride-specific gait parameters have been linked directly with disease onset and progression [3–9]. Therefore, stride time, stance time, and swing time were calculated, and the differences between the deep learning-based approach and the marker-based reference method were quantified (Table 5, Figure 3). The limits of agreement for a 95% confidence interval were calculated, and for all metrics the zero mean difference was enclosed in the limit of agreement.

5. Conclusions

In this study we have validated a deep learning-based approach to detect gait events and subsequently extract clinically relevant stride parameters from a single inertial measurement unit. Performance analysis showed an excellent detection rate, and low time errors in both event detection and stride parameter calculation for different walking speeds and across both healthy and neurological cohorts. Our next step is to validate these methods under more challenging conditions, that involve real-life walking sequences.

Author Contributions: Conceptualization, R.R., G.S., and W.M.; methodology, R.R., G.S.; software, R.R.; validation, R.R.,; formal analysis, R.R.; investigation, R.R., G.S., W.M.; resources, C.H, W.M..; data curation, E.W., R.R.,; writing—original draft preparation, R.R.; writing—review and editing, E.W., C.H., G.S., W.M.; visualization, R.R.; supervision, G.S., W.M.; project administration, R.R., E.W., C.H., G.S., W.M.; funding acquisition, W.M. All authors have read and agreed to the published version of the manuscript.

Funding: This research received funding from the DFG Open Access fund.

Institutional Review Board Statement: The study was conducted in accordance with the Declaration of Helsinki, and approved by the Ethics Committee of the medical faculty of the Christian-Albrechts-Universität zu Kiel (D438/18, approved on 8 May 2018).

Informed Consent Statement: Informed consent was obtained from all subjects involved in the study.

Data Availability Statement: Data from the first 10 participant are available online at https://github.com/neurogeriatricskiel/Validation-dataset. Additionally, we are preparing the open-source release of all data from the healthy younger and older adults. Data from ptient groups

Acknowledgments: The authors sincerely thank all people that were involved in the data collection, from study participants to students who aided and assisted during measurements and subsequent marker labeling. The authors appreciate the off- and on-topic discussions with Julius Welzel, and his positive contributions to the organization of the research data. The authors give a thumbs up to Johannes Hoffmann for his tips and tricks regarding the LaTeXtypesetting.

Conflicts of Interest: The authors declare no conflict of interest.

Abbreviations

The following abbreviations are used in this manuscript:

cLBP	chronic low back pain
CNN	convolutional neural network
IMU	inertial measurement unit
MS	multiple sclerosis
OA	older adults
PD	Parkinson's Disease
TCN	temporal convolutional network
YA	younger adults

References

1. Snijders, A.H.; van de Warrenburg, B.P.; Giladi, N.; Bloem, B.R. Neurological gait disorders in elderly people: clinical approach and classification. *Lancet Neurol.* **2007**, *6*(1), 63–74.
2. Hodgins, D. The importance of measuring human gait. *Med. Device Technol.* **2008**, *19*(5):42, 44-7.
3. Del Din, S.; Elshehabi, M.; Galna, B.; Hobert, M.A.; Warmerdam, E.; Suenkel, U.; Brockmann, K.; Metzger, F.; Hansen, C.; Berg, D.; Rochester, L.; Maetzler, W. Gait analysis with wearables predicts conversion to Parkinson disease. *Ann. Neurol.* **2019**, *86*(3), 357–367.
4. König, A.; Klaming, L.; Pijl, M.; Demeurraux, A.; Davis, R.; Robert, P. Objective measurement of gait parameters in healthy and cognitively impaired elderly using the dual-task paradigm. *Aging. Clin. Exp. Res.* **2017**, *29*(6), 1181–1189.
5. Bertoli, M.; Cereatti, A.; Trojaniello, D.; Avanzino, L.; Pelosin, E.; Del Din, S.; Rochester, L.; Ginis, P.; Bekkers, E.M.J.; Mirelman, A.; Hausdorff, J.M.; Della Croce, U. Estimation of spatio-temporal parameters of gait from magneto-inertial measurement units: multicenter validation among Parkinson, mildly cognitively impaired and healthy older adults. *Biomed. Eng. Online* **2018**, *17*(58).
6. von Schroeder, H.P.; Coutts, R.D.; Lyden, P.D.; Billings, E., Jr; Nickel, V. L. Gait parameters following stroke: a practical assessment. *J. Rehabil. Res. Dev.* **1995**, *32*(1), 25–31.
7. Mohan, D.M.; Khandoker, A.H.; Wasti, S.A.; Ismail Ibrahim Ismail Alali, S.; Jelinek, H.F.; Khalaf, K. Assessment methods of post-stroke gait: A scoping review of technology-driven approaches to gait characterization and analysis. *Front. Neurol.* **2021**, *12*.
8. Griškevičius, J.; Apanskienė, V.; Žižienė, J.; Daunoravičienė, K.; Ovčinikova, A.; Kizlaitienė, R.; Sereikė, I.; Kaubrys, G.; Pauk, J.; Idźkowski, A. Estimation of temporal gait parameters of multiple sclerosis patients in clinical setting using inertial sensors. In Proceedings of the 11th Int Conf BIOMDLORE 2016, Druskininkai, Lithuania, 20–22 Oct 2016; 80–82.
9. Flachenecker, F.; Gaßner, H.; Hannik, J.; Lee, D.H.; Flachenecker, P.; Winkler, J.; Eskofier, B.; Linker, R.A.; Klucken, J. Objective sensor-based gait measures reflect motor impairment in multiple sclerosis patients: Reliability and clinical validation of a wearable sensor device. *Mult. Scler. Relat. Dis.* **2019**, *39*, 101903.
10. Hannink, J.; Kautz, T.; Pasluosta, C.F.; Gaßmann, K.-G.; Klucken, J.; Eskofier, B.M. Sensor-Based Gait Parameter Extraction With Deep Convolutional Neural Networks. *IEEE J. Biomed. Health* **2017**, *21*(1), 85–93.
11. Perry, J; Burnfield, J.M. *Gait analysis: normal and pathological gait*, 2nd ed.; SLACK Inc.: Thorofare, NJ, USA, 2010.
12. Richards, J.; Levine, D.; Whittle, M. *Whittle's Gait Analysis*, 5th ed.; Churchill Livingstone: London, UK, 2012.
13. Rueterbories, J.; Spaich, E.G.; Larsen, B.; Andersen, O.K. Methods for gait event detection and analysis in ambulatory systems. *Med. Eng. Phys.* **2010**, *32*(6), 545–552.
14. Bruening, D.A.; Ridge, S.T. Automated event detection algorithms in pathological gait. *Gait Posture* **2014**, *39*(1), 472–477.
15. Chiari, L.; Della Croce, U.; Leardini, A.; Cappozzo, A. Human movement analysis using stereophotogrammetry: Part 2: Instrumental errors *Gait Posture* **2005**, *21*(2), 197–211.
16. Topley, M.; Richards, J.G. A A comparison of currently available optoelectronic motion capture systems. *J. Biomech.* **2020**, *106*:109820.
17. Iosa, M.; Picerno, P.; Paolucci, S.; Morone, G. Wearable inertial sensors for human movement analysis. *Expert Rev. Med. Devic.* **2016**, *13*(7), 641–659.
18. Jarchi, D.; Pope, J.; Lee, T.K.M.; Tamjidi, L.; Mirzaei, A.; Sanei, S. A Review on Accelerometry-Based Gait Analysis and Emerging Clinical Applications. *IEEE Rev. Biomed. Eng.* **2018**, *11*, 177–194.
19. Hillel, I; Gazit, E.; Nieuwboer, A.; Avanzino, L.; Rochester, L.; Cereatti, A.; Della Croce, U.; Rikkert, M.O.; Bloem, B.R.; Pelosin, E.; Del Din, S.; Ginis, P.; Giladi, N.; Mirelman, A.; Hausdorff, J.M. Is every-day walking in older adults more analogous to dual-task walking or to usual walking? Elucidating the gaps between gait performance in the lab and during 24/7 monitoring. *Eur. Rev. Aging Phys. A.* **2019**, *16*(6).
20. Warmerdam, E.; Hausdorff, J.M.; Atrsaei, A.; Zhou, Y.; Mirelman, A.; Aminian, K.; Espay, A.J.; Hansen, C.; Evers, L.J.W.; Keller, A.; Lamoth, C.; Pilotto, A.; Rochester, L.; Schmidt, G.; Bloem, B.R.; Maetzler, W. Long-term unsupervised mobility assessment in movement disorders. *Lancet Neurol.* **2020**, *19*(5), 462–470.
21. Atrsaei, A.; Corrá, M.F.; Dadashi, F.; Vila-Chã, N.; Maia, L.; Mariani, B.; Maetzler, W.; Aminian, K. Gait speed in clinical and daily living assessments in Parkinson's disease patients: performance versus capacity. *npj Parkinsons Dis.* **2021**, *7*(1):24.
22. Del Din, S.; Godfrey, A.; Mazzà, C.; Lord, S.; Rochester, L. Free-living monitoring of Parkinson's disease: Lessons from the field. *Movement Disord.* **2016**, *31*(9), 1293–1313.
23. Shah, V.V.; McNames, J.; Mancini, M.; Carlson-Kuhta, P.; Nutt, J.G.; El-Gohary, M.; Lapidus, J.A.; Horak, F.B.; Curtze, C. Digital Biomarkers of Mobility in Parkinson's Disease During Daily Living. *J. Parkinson Dis.* **2020**, *10*(3), 1099–1111.

24. Fasano, A.; Mancini, M. Wearable-based mobility monitoring: the long road ahead. *Lancet Neurol.* **2020**, *19*(5), 378–379.
25. Corrá, M.F.; Atrsaei, A.; Sardoreira, A.; Hansen, C.; Aminian, K.; Correia, M.; Vila-Chã, N.; Maetzler, W.; Maia, L. Comparison of Laboratory and Daily-Life Gait Speed Assessment during ON and OFF States in Parkinson's Disease. *Sensors* **2021**, *21*(12):3974.
26. Ben Mansour, K.; Rezzoug, N.; Gorce, P. Analysis of several methods and inertial sensors locations to assess gait parameters in able-bodied subjects. *Gait Posture* **2015**, *42*, 409–414.
27. Storm, F.A.; Buckley, C.J.; Mazzà, C. Gait event detection in laboratory and real life settings: Accuracy of ankle and waist sensor based methods. *Gait Posture* **2016**, *50*, 42–46.
28. Panebianco, G.P.; Bisi, M.C.; Stagni, R.; Fantozzi, S. Analysis of the performance of 17 algorithms from a systematic review: Influence of sensor position, analysed variable and computational approach in gait timing estimation from IMU measurements. *Gait Posture* **2018**, *66*, 76–82.
29. Niswander, W.; Kontson, K. Evaluating the Impact of IMU Sensor Location and Walking Task on Accuracy of Gait Event Detection Algorithms. *Sensors* **2021**, *21*(12):3989.
30. Salarian, A.; Russmann, H.; Vingerhoets, F.J.; Dehollain, C.; Blanc, Y.; Burkhard, P.R.; Aminian, K. Gait assessment in Parkinson's disease: Toward an ambulatory system for long-term monitoring. *IEEE Trans. Biomed. Eng.* **2004**, *51*(8), 1434–1443.
31. Catalfamo, P.; Ghoussayni, S.; Ewins, D. Gait Event Detection on Level Ground and Incline Walking Using a Rate Gyroscope. *Sensors* **2010**, *10*(6), 5683–5702.
32. Sabatini, A.; Martelloni, C.; Scapellato, S.; Cavallo, F. Assessment of Walking Features from Foot Inertial Sensing. *IEEE Trans. Biomed. Eng.* **2005**, *52*(3), 486–494.
33. Maqbool, H.F.; Husman, M.A.B.; Awad, M.; Abouhossein, A.; Mehryar, P.; Iqbal, N.; Dehghani-Sanij, A.A. Real-time gait event detection for lower limb amputees using a single wearable sensor. In Proceedings of the 2016 38th Ann. Int. Conf. of the IEEE Eng. in Med. Biol. Soc. (EMBC), Orlando, FL, USA, 16–20 Aug. 2016, IEEE: Piscataway, NJ, USA, 2016.
34. Romijnders, R.; Warmerdam, E.; Hansen, C.; Welzel, J.; Schmidt, G.; Maetzler, W. Validation of IMU-based gait event detection during curved walking and turning in older adults and Parkinson's Disease patients. *J. Neuroeng. Rehabil.* **2021**, *18*:28.
35. Jasiewicz, J.M.; Allum, J.H.; Middleton, J.W.; Barriskill, A.; Condie, P.; Purcell, B.; Li, R.C.T. Gait event detection using linear accelerometers or angular velocity transducers in able-bodied and spinal-cord injured individuals. *Gait Posture* **2006**, *24*(4), 502–509.
36. Trojaniello, D.; Cereatti, A.; Pelosin, E.; Avanzino, L.; Mirelman, A.; Hausdorff, J.M.; Della Croce, U. Estimation of step-by-step spatio-temporal parameters of normal and impaired gait using shank-mounted magneto-inertial sensors: Application to elderly, hemiparetic, parkinsonian and choreic gait. *J. Neuroeng. Rehabil.* **2014**, *11*:152.
37. Ferraris, F.; Grimaldi, U.; Parvis, M. Procedure for effortless in-field calibration of three-axis rate gyros and accelerometers. *Sensor. Mater.* **1995**, *7*(5), 311–330.
38. Greene, B.R.; McGrath, D.; O'Neill, R.; O'Donovan, K.J.; Burns, A.; Caulfield, B. An adaptive gyroscope-based algorithm for temporal gait analysis. *Med. Biol. Eng. Comput.* **2010**, *48*(12), 1251–1260.
39. LeCun, Y.; Bengio, Y.; Hinton, G. Deep learning. *Nature* **2015**, *521*, 436-444.
40. Ter Haar Romeny, B.M. A Deeper Understanding of Deep Learning. In *Artificial Intelligence in Medical Imaging: Opportunities, Applications and Risks*; Ranschaert, E.R., Morozov, S., Algra, P.R., Eds.; Springer Int. Publish.: Cham, Switzerland, 2019; pp. 25–38.
41. Kidziński, Ł.; Delp, S.; Schwartz, M. Automatic real-time gait event detection in children using deep neural networks. *PLoS ONE* **2019**, *14*(1):e0211466.
42. Lempereur, M.; Rousseau, F.; Rémy-Néris, O.; Pons, C.; Houx, L.; Quellec, G.; Brochard, S. A new deep learning-based method for the detection of gait events in children with gait disorders: Proof-of-concept and concurrent validity. *J. Biomech.* **2020**, *98*, 109490.
43. Filtjens, B.; Nieuwboer, A.; D'cruz, N.; Spildooren, J.; Slaets, P.; Vanrumste, B. A data-driven approach for detecting gait events during turning in people with Parkinson's disease and freezing of gait. *Gait Posture* **2020**, *80*, 130–136.
44. Gadaleta, M.; Cisotto, G.; Rossi, M.; Ur Rehman, R.Z.; Rochester, L.; Del Din, S. Deep Learning Techniques for Improving Digital Gait Segmentation. In Proceedings of the 2019 41st Ann. Int. Conf. of the IEEE Eng. in Med. Biol. Soc. (EMBC), Berlin, Germany, 23–27 Jul. 2019, IEEE: Piscataway, NJ, USA, 2019.
45. Warmerdam, E.; Romijnders, R.; Geritz, J.; Elshehabi, M.; Maetzler, C.; Otto, J.C.; Reimer, M.; Stuerner, K.; Baron, R.; Paschen, S.; Beyer, T.; Dopcke, D.; Eiken, T.; Ortmann, H.; Peters, F.; von der Recke, F.; Riesen, M.; Rohwedder, G.; Schaade, A.; Schumacher, M.; Sondermann, A; Maetzler, W.; Hansen, C. Proposed Mobility Assessments with Simultaneous Full-Body Inertial Measurement Units and Optical Motion Capture in Healthy Adults and Neurological Patients for Future Validation Studies: Study Protocol. *Sensors* **2021**, *21*(17):5833.
46. Gibb, W.R.; Lees, A.J. The relevance of the Lewy body to the pathogenesis of idiopathic Parkinson's disease. *J. Neurol. Neurosur. Ps.* **1988**, *51*(6), 745–752.
47. Thompson, A.J.; Banwell, B.L.; Barkhof, F.; Carroll, W.M.; Coetzee, T.; Comi, G.; Correale, J.; Fazekas, F.; Filippi, M.; Freedman, M.S.; Fujihara, K.; Galetta, S.L.; Hartung, H.P.; Kappos, L.; Lublin, F.D.; Marrie, R.A.; Miller, A.E.; Miller, D.H.; Montalban, X.; Mowry, E.M.; Soelberg Sorensen, P.; Tintoré, M.; Traboulsee, A.L.; Trojano, M.; Uitdehaag, B.M.J.; Vukusic, S.; Waubant, E.; Weinshenker, B.G.; Reingold, S.C.; Cohen, J.A. Diagnosis of multiple sclerosis: 2017 revisions of the McDonald criteria. *Lancet Neurol.* **2018**, *17*(2), 162–173.

48. Nasreddine, Z.S.; Phillips, N.A.; Bédirian, V.; Charbonneau, S.; Whitehead, V.; Collin, I.; Cummings, J.L.; Chertkow, H. The Montreal Cognitive Assessment, MoCA: A Brief Screening Tool For Mild Cognitive Impairment. *J. Am. Geriatr. Soc.* **2005**, *53*(4), 695–699.
49. Federolf, P.A. A Novel Approach to Solve the "Missing Marker Problem" in Marker-Based Motion Analysis That Exploits the Segment Coordination Patterns in Multi-Limb Motion Data. *PLoS ONE* **2013**, *8*(10), 1–13.
50. Gløersen, Ø; Federolf, P. Predicting Missing Marker Trajectories in Human Motion Data Using Marker Intercorrelations. *PLoS ONE* **2016**, *11*(3), 1–14.
51. Kormylo, J.; Jain, V. Two-pass recursive digital filter with zero phase shift. *IEEE T. Acoust. Speech* **1974**, *22*(5), 384–387.
52. Rácz, K.; Rita, M.K. Marker displacement data filtering in gait analysis: A technical note. *Biomed. Signal Proces.* **2021**, *70*:102974.
53. Pijnappels, M.; Bobbert, M.F.; Van Dieën, J.H. Changes in walking pattern caused by the possibility of a tripping reaction. *Gait Posture* **2001**, *14*(1), 11–18.
54. O'Connor, C.M.; Thorpe, S.K.; O'Malley, M.J.; Vaughan, C.L. Automatic detection of gait events using kinematic data. *Gait Posture* **2007**, *25*(3), 469–474.
55. Carcreff, L.; Gerber, C.; Paraschiv-Ionescu, A.; De Coulon, G,; Newman, C.; Armand, S.; Aminian, K. What is the best configuration of wearable sensors to measure spatiotemporal gait parameters in children with cerebral palsy? *Sensors* **2018**, *18*(2):394.
56. Yu, F.; Koltun, V. Multi-Scale Context Aggregation by Dilated Convolutions. In Proceedings of the 4th Int. Conf. on Learning Representations (ICLR), San Juan, Puerto Rico, 2–4 May 2016, Conference Track Proceedings, 2016.
57. Bai, S.; Kolter, J.Z.; Koltun, V. An Empirical Evaluation of Generic Convolutional and Recurrent Networks for Sequence Modeling. *arXiv:1803.01271* **2018**.
58. Rémy, P. Temporal Convolutional Networks for Keras. *GitHub repository* **2020**, *GitHub*, https://github.com/philipperemy/keras-tcn.
59. LeCun, Y.; Boser, B.; Denker, J.S.; Henderson, D.; Howard, R.E.; Hubbard, W.; Jackel, L.D. Backpropagation Applied to Handwritten Zip Code Recognition. *Neural Comput.* **1989**, *1*(4), 541–551.
60. Ioffe, S.; Szegedy, C. Batch Normalization: Accelerating Deep Network Training by Reducing Internal Covariate Shift. *arXiv:1502.03167* **2015**.
61. Srivastava, N.; Hinton, G.; Krizhevsky, A.; Sutskever, I.; Salakhutdinov, R. Dropout: a simple way to prevent neural networks from overfitting. *J. Mach. Learn. Res.* **2014** *15*, 1929–1958.
62. van den Oord, A.; Dieleman, S.; Zen, H.; Simonyan, K.; Vinyals, O.; Graves, A.; Kalchbrenner, N.; Senior, A.W.; Kavukcuoglu, K. WaveNet: A generative model for raw audio. *arXiv:1609.03499* **2016**.
63. O'Malley, T.; Bursztein, E.; Long, J.; Chollet, F.; Jin, H.; Invernizzi, L.; and others; KerasTuner. *GitHub repository* **2019**, *GitHub*, https://github.com/keras-team/keras-tuner.
64. Kingma, D.P.; Ba, J. Adam: A Method for Stochastic Optimization *arXiv:1412.6980v9* **2014**.
65. Schmidt, R.M.; Schneider, F.; Henning, P. Descending through a crowded valley-benchmarking deep learning optimizers. In Proceedings of the 38th Int. Conf. on Machine Learning (ICML), *online*, 18–24 Jul. 2021, pp. 9367–9376.
66. Bergstra, J.; Bengio, Y. Random Search for Hyper-Parameter Optimization. *J. Mach. Learn. Res.* **2012**, *13*(10), 281–305.
67. Mishra, P.; Pandey, C.M.; Singh, U.; Gupta, A.; Sahu, C.; Keshri, A. Descriptive Statistics and Normality Tests for Statistical Data. *Ann. Card. Anaesth.* **2019**, *22*(1), 67–72.
68. Wilcoxon, F. Individual Comparisons by Ranking Methods. *Biometrics Bull.* **1945**, *1*, 80–83.
69. McDonald, J.H. *Handbook of Biological Statistics*, 3rd ed.; Sparky House Publishing: Sparky House Publishing, USA, 2014; pp. 186–189.
70. Diez, D.; Çetinkaya-Rundel, M.; Barr, C.D. *OpenIntro Statistics*, 4th ed.; 2019. https://www.openintro.org/book/os/